

A high-throughput small molecule screen identifies synergism between DNA methylation and Aurora kinase pathways for X reactivation

Derek Lessing^{a,b,c,1}, Thomas O. Dial^{a,b,c,1}, Chunyao Wei^{a,b,c}, Bernhard Payer^d, Lieselot L. G. Carrette^{a,b,c,e}, Barry Kesner^{a,b,c}, Attila Szanto^{a,b,c}, Ajit Jadhav^f, David J. Maloney^f, Anton Simeonov^f, Jimmy Theriault^g, Thomas Hasaka^g, Antonio Bedalov^h, Marisa S. Bartolomeiⁱ, and Jeannie T. Lee^{a,b,c,2}

^aHoward Hughes Medical Institute, Massachusetts General Hospital, Boston, MA 02114; ^bDepartment of Molecular Biology, Massachusetts General Hospital, Boston, MA 02114; ^cDepartment of Genetics, Harvard Medical School, Boston, MA 02115; ^dCentre for Genomic Regulation, 08003 Barcelona, Spain; ^eCenter for Medical Genetics, Ghent University, 9000 Ghent, Belgium; ^fDivision of Preclinical Innovation, National Center for Advancing Translational Sciences, National Institutes of Health, Rockville, MD 20850; ^gBroad Institute, Cambridge, MA 02142; ^hClinical Research Division, Fred Hutchinson Cancer Research Center, Seattle, WA 98109; and ⁱDepartment of Cell and Developmental Biology, University of Pennsylvania School of Medicine, Philadelphia, PA 19104

Contributed by Jeannie T. Lee, October 28, 2016 (sent for review July 29, 2016; reviewed by Sanchita Bhatnagar, Joost Gribnau, Jeanne B. Lawrence, and Lucy Williams)

X-chromosome inactivation is a mechanism of dosage compensation in which one of the two X chromosomes in female mammals is transcriptionally silenced. Once established, silencing of the inactive X (Xi) is robust and difficult to reverse pharmacologically. However, the Xi is a reservoir of >1,000 functional genes that could be potentially tapped to treat X-linked disease. To identify compounds that could reactivate the Xi, here we screened ~367,000 small molecules in an automated high-content screen using an Xi-linked GFP reporter in mouse fibroblasts. Given the robust nature of silencing, we sensitized the screen by “priming” cells with the DNA methyltransferase inhibitor, 5-aza-2'-deoxycytidine (5azadC). Compounds that elicited GFP activity include VX680, MLN8237, and 5azadC, which are known to target the Aurora kinase and DNA methylation pathways. We demonstrate that the combinations of VX680 and 5azadC, as well as MLN8237 and 5azadC, synergistically up-regulate genes on the Xi. Thus, our work identifies a synergism between the DNA methylation and Aurora kinase pathways as being one of interest for possible pharmacological reactivation of the Xi.

X reactivation | high-throughput screen | small molecules | Aurora kinase | DNA methyltransferase

Female mammals are subject to a form of epigenetic regulation termed X-chromosome inactivation (XCI), in which one of the two X chromosomes is transcriptionally silenced to avoid gene dosage imbalance compared with males (1–3). As a result of this process, in any particular female cell an X-linked gene's function is provided solely by one of its two alleles. XCI has been intensively investigated over the past 55 years and a number of regulatory factors have now been identified. These factors include long noncoding RNAs (lncRNAs) that mediate X-chromosome counting, allelic choice, and initiation of silencing, as well as protein factors that interact with the lncRNAs to effect each of these steps of silencing. XCI is observed in three contexts *in vivo* in mice (4). In the male germline, the X and Y chromosomes are inactivated together during pachytene of the first meiotic prophase (5). In the preimplantation embryo, the paternally inherited X chromosome is inactive as a consequence of imprinting (6). Finally, in the epiblast lineage, a random XCI process occurs after the paternal X is reactivated (7).

Whereas XCI has been studied extensively, X-chromosome reactivation (XCR) has been less amenable to molecular analysis and its underlying mechanisms remain poorly understood (8–10). XCR occurs naturally in two contexts. At embryonic day 4.0 (E4.0), the imprinted form of XCI is reversed and this paternal X reactivation results in a transient state in which two active X chromosomes (Xa's) are present in the epiblast lineage (7). As the embryo differentiates into three germ layers, random XCI

initiates for one of the two X chromosomes (11), a process that begins with the expression of the noncoding RNA, “X-inactive specific transcript” or Xist, from the future inactive X chromosome (Xi) (12) and continues with the recruitment of chromatin modification factors such as Polycomb repressive complex 2 (13–15). The same Xi then remains silenced for all subsequent cell divisions throughout the life of the mouse—with the exception of the germ cell lineage, in which XCI is once again reversed before female meiosis (16, 17). Thus, during mouse development, multiple rounds of XCI and XCR occur.

Once silencing is established, the Xi is extremely robust and becomes difficult to reactivate outside of the normal developmental context, due to multiple parallel mechanisms of silencing involving Polycomb complexes and histone H3 lysine 27 trimethylation, incorporation of variant histones, hypoacetylation of histone tails, and increased DNA methylation (1–3, 18). However, the Xi harbors genes that could in principle be reactivated to treat X-linked diseases, such as Rett syndrome and cyclin-dependent kinase-like 5 (CDKL5) syndrome, two neurodevelopmental disorders affecting girls who are heterozygous for mutations in methyl CpG binding protein 2 (*MECP2*) and *CDKL5*,

Significance

In mammalian female cells, nearly all genes are silenced on one of two X chromosomes. Heterozygous females with “dominant” X-linked diseases, such as Rett syndrome, may benefit from pharmacological reactivation of the silent, healthy allele in affected organs. Toward establishing proof of concept, here we carry out a primed screen of a large library of small molecules for compounds that can reactivate expression from the inactive X (Xi). We identify a combination of compounds that inhibits the DNA methylation and Aurora kinase pathways and demonstrate that the two pathways act synergistically to repress genes on the Xi, including genes involved in X-linked disease.

Author contributions: D.L., T.O.D., B.P., and J.T.L. designed research; D.L., T.O.D., C.W., B.P., L.L.G.C., A. Szanto, J.T., and T.H. performed research; A.J., D.J.M., A. Simeonov, A.B., and M.S.B. contributed new reagents/analytic tools; D.L., T.O.D., C.W., B.P., L.L.G.C., B.K., A. Szanto, A.J., J.T., T.H., and J.T.L. analyzed data; and D.L., T.O.D., and J.T.L. wrote the paper.

Reviewers: S.B., University of Virginia; J.G., Erasmus Medical Center; J.B.L., University of Massachusetts Medical Center; and L.W., University of North Carolina-Chapel Hill.

Data deposition: The complete primary screen data have been deposited in the PubChem database, pubchem.ncbi.nlm.nih.gov (accession no. [AID 743238](https://pubchem.ncbi.nlm.nih.gov/compound/AID743238)). The sequence read data have been deposited into the Gene Expression Omnibus (GEO) database (accession no. [GSE85103](https://www.ncbi.nlm.nih.gov/geo/query/acc.cgi?acc=GSE85103)).

¹D.L. and T.O.D. contributed equally to this work.

²To whom correspondence should be addressed. Email: lee@molbio.mgh.harvard.edu.

This article contains supporting information online at www.pnas.org/lookup/suppl/doi:10.1073/pnas.1617597113/-DCSupplemental.

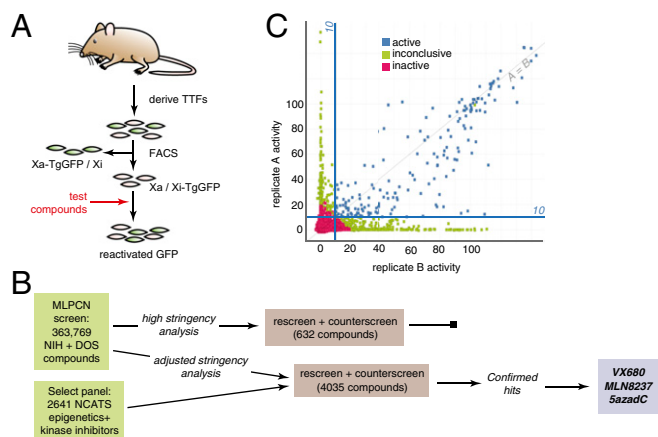


Fig. 1. Summary of X-reactivation screen of small molecules. (A) Derivation of Xi-TgGFP cells from TTFs isolated from pups heterozygous for the X-linked GFP transgene. (B) Steps of the screening process. Initial analysis identified 632 compounds (199 active + 433 inconclusive, C) that subsequently failed rescreening. Reanalysis of the primary screen data identified 1,895 compounds not among the initial 632; 1,394 of these were sourced for rescreening along with an additional 2,641 test compounds. Of 15 compounds that passed this stage, confirmation by qRT-PCR was obtained only for VX680, MLN8237, and 5azadC (Methods and Fig. 2). (C) Primary screen results. The two replicates are plotted against each other on a normalized 0–100 scale. Blue lines indicate the threshold of 10 for active compounds on each axis.

respectively (19, 20). In recent years, several approaches have been taken to define a pharmacological means of reactivating the Xi in somatic cells. Two siRNA screens led to identification of a number of factors, but the screens obtained divergent results with no overlap (21, 22). Possible explanations for this are that the screens might not have been fully comprehensive or that XCI cannot be robustly overcome by disrupting a single factor. Another screen involving siRNAs and a limited collection of small molecules identified ribonucleoside-diphosphate reductase subunit M2 (*RRM2*) as being synergistic with 5-aza-2'-deoxycytidine for reactivation of the Xi (23). In yet another approach, Xist RNA was used as bait to pull down interacting proteins, a number of which could be targeted using small molecules to reactivate the Xi (15). It was demonstrated that derepression of the Xi can be achieved robustly only when two or more interactors were targeted. Although >100 interacting proteins were identified, most of the interactors are not druggable with small molecules. Thus, additional approaches are needed to maximize the potential for pharmaceutical intervention. With this in mind, here we undertake an unbiased approach and perform a high-throughput small molecule screen to identify compounds that will reactivate a reporter transgene on the Xi.

Results

A High-Throughput Screen for X Reactivation. We developed a female mouse fibroblast cell line, Xi-TgGFP, in which the Xi carries a silent GFP transgene (24) as a reporter for reactivation (Fig. 1A). Using the Xi-TgGFP cell line, we screened >367,000 molecules, combining compounds from the NIH's Molecular Libraries Program, the Broad Institute's Diversity-Oriented Synthesis Library, and a panel of kinase and epigenetic inhibitors from the National Center for Advancing Translational Sciences (NCATS) (Fig. 1B). Because previous work demonstrated that the Xi is repressed by multiple synergistic mechanisms (15, 18), we reasoned that the odds of success would be increased by performing a primed screen in which cells were sensitized to derepression with the DNA methylation inhibitor, 5-aza-2'-deoxycytidine (5azadC), a compound shown previously to elicit a very low level of Xi reactivation (18). We chose a priming concentration of 0.5 μ M 5azadC, empirically determined to yield ~1% GFP⁺ cells, a value that was just above background levels (Fig. S1).

GFP reactivation in the Xi-TgGFP cells was scored in the high-throughput, primed screen via automated microscopy, after a 3-day treatment with each compound tested in duplicate at 7.5 μ M with 5azadC priming. We found ~1,900 compounds that reactivated GFP in at least 10% of cells (on a normalized scale) (Methods). We resourced ~1,400 of these and repeated the GFP reactivation assay at 5.0 μ M and 0.5 μ M (both concentrations with 0.5 μ M 5azadC) alongside a counterscreen for autofluorescence (i.e., false-positive GFP signal). Almost all were either autofluorescent or too toxic. The Aurora kinase inhibitors VX680 (25) and MLN8237 (26) were chosen for further studies, as detailed below.

Synergism Between VX680, MLN8237, and 5azadC. The Aurora kinase family consists of Aurora kinase A (AURKA), B (AURKB), and C (AURKC). Whereas AURKA and AURKB are ubiquitously expressed, AURKC is expressed only in the testis (27) and was therefore not likely to be relevant as a target here. AURKA was also recently identified in an shRNA screen for X reactivators using a similar X-reactivation assay (22), and AURKB was identified as a protein that directly interacts with Xist RNA (15).

Application of VX680 in the screen led to a 23.5% GFP-reactivation average of two replicates (Fig. S1C). We reproduced its reactivation via an independent assay, in which we used quantitative RT-PCR (qRT-PCR) to measure GFP expression (Fig. 2A). VX680 alone boosted GFP expression by 6.6-fold and, when combined with 5azadC, by 4.3-fold over treatment with 5azadC alone. We compared this expression to that of a male fibroblast line carrying the GFP transgene on the single, active X chromosome (Xa-TgGFP), which represents the theoretical maximum for GFP activity on the X chromosome. When normalized to male Xa-TgGFP expression, the response of VX680 and 5azadC reached 13% of the theoretical maximum (15, 18).

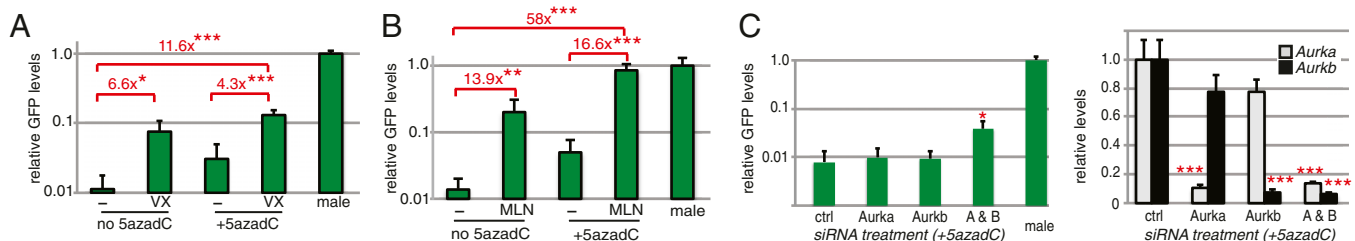


Fig. 2. GFP reactivation by Aurora kinase inhibitors, VX680 and MLN8237. (A) Xi-TgGFP female fibroblasts were treated for 3 d with VX680 at 1 μ M, 5azadC at 0.5 μ M, or both. Expression is relative to X-TgGFP/Y male cells. Means \pm SD of three to five biological replicates are shown. Note that the y axis is a logarithmic scale. Fold differences vs. controls are indicated in red; * P = 0.02, *** P < 0.001. (B) The same cells were treated with 1 μ M MLN8237 and tested as in A. ** P = 0.01; *** P < 0.001. (C) Xi-TgGFP cells treated with control, *Aurka*, *Aurkb*, or both *Aurka* and *Aurkb* siRNAs. (Left) qRT-PCR of GFP expression, mean RNA levels \pm SD, * P = 0.02. Note logarithmic scale on y axis. (Right) Knockdown efficiency of each *Aurk* gene assessed by qRT-PCR, *** P < 0.001.

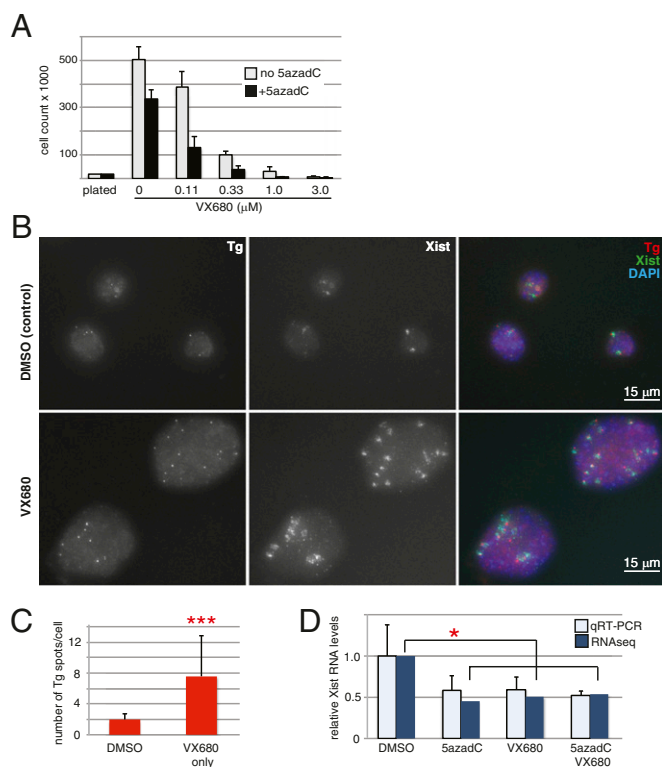


Fig. 3. VX680 effects on cell proliferation and Xist RNA. (A) A total of 20,000 cells were plated per well in 12-well plates ("plated" on x axis). After 3-d treatment with indicated concentrations, viable cells were counted. Means of three experiments \pm SD are shown. (B, Left) DNA FISH with probe for GFP transgene (Tg). (Center) RNA FISH with probe for Xist. (Right) Merged images include DAPI stain of nuclei. (Top) FISH of control cells treated with DMSO. (Bottom) FISH of cells treated with 1 μ M VX680 for 3 d. (C) Quantification of GFP transgene signals from DNA FISH experiments. *** $P < 0.001$. (D) Relative amounts of Xist RNA upon 3-d treatment with 0.5 μ M 5azadC, 1 μ M VX680, or both, shown by qRT-PCR or by a fold-change calculation from RNA-seq data (*FDR < 0.05 for each drug treatment compared with the DMSO control).

Included in our screen were 28 other Aurora kinase inhibitors apart from VX680. Whereas none elicited GFP-reactivation activity within an acceptable level of cell toxicity (Table S1), MLN8237 was confirmed with even greater reactivation activity than VX680 in the GFP qRT-PCR assay (Fig. 2B). MLN8237 at 1 μ M elicited 13.9-fold activity by itself. When combined with 5azadC, it yielded a 16.6-fold reactivation level over 5azadC alone; this was 83.5% of the male Xa-TgGFP control (Fig. 2B). MLN8237 is a more specific AURKA inhibitor than VX680 ($IC_{50} = 7$ nM for AURKA in a cell culture assay, vs. 1,500 nM for AURKB) (28). Combined, our findings implicate the Aurora kinase pathway as one of potential significance for pharmacological X reactivation.

AURKA and AURKB Knockdown Partially Recapitulates VX680- and MLN8237-Induced Reactivation of GFP. Next, we sought to determine whether AURKA and AURKB are the relevant targets of VX680 and MLN8237 for X reactivation. VX680 and MLN8237 (28, 29) can affect other protein kinases as well (30–32) (Table S2). We directly tested the roles of *Aurka* and *Aurkb* in reactivation by knocking down their expression with siRNAs alone or together. Each was efficiently knocked down to $\sim 10\%$ of normal levels (Fig. 2C). Aurora kinase knockdown alone led to no increase in GFP expression. In the presence of 0.5 μ M 5azadC, knockdown of either AURKA or AURKB individually also did not result in increased GFP transcription. However, with simultaneous knockdown, GFP expression increased 4.8-fold relative to 5azadC treatment by

itself. Because this level was just 4% of Xa-TgGFP levels, compared with 13% for VX680 or 83% for MLN8237, VX680- and MLN8237-mediated reactivation can be attributed only in part to AURKA and AURKB. Whereas residual Aurora kinase activity after knockdown may be greater than after inhibition by VX680 or MLN8237, it is also possible that these compounds target additional kinases to achieve their full effect on X reactivation.

Additional Effects of VX680. During mitosis, AURKA is necessary for proper centrosome maturation, spindle assembly, and centrosome separation. AURKB is a member of the chromosomal passenger complex, which phosphorylates histone H3 and other substrates for proper cytokinesis (27). Lack of AURKA function is known to have a severe effect on cell cycle progression and to cause lethality before implantation, whereas lack of AURKB is known to be lethal after implantation and to cause errors in chromosome segregation (33). Therefore, we further examined effects of Aurora kinase inhibition on general cellular processes. As expected, cell proliferation was inhibited by VX680 in a dose-dependent manner; this toxicity was similar with or without 5azadC, consistent with the known effects of Aurora kinase inhibition on cell division (Fig. 3A).

Work on Aurora kinases has shown that dividing cells lacking both kinases exit mitosis before anaphase and give rise to aneuploid daughters (34). We therefore considered the possibility that apparent GFP reactivation might be an artifact of this. We first looked at Xist expression and localization by FISH after treating cells with VX680 alone to focus on its mitotic effects. Interestingly, cells treated with 1 μ M VX680 developed nuclei more than five times the size of control-treated nuclei (Fig. 3B). Furthermore, the VX680-treated cells exhibited an excessive

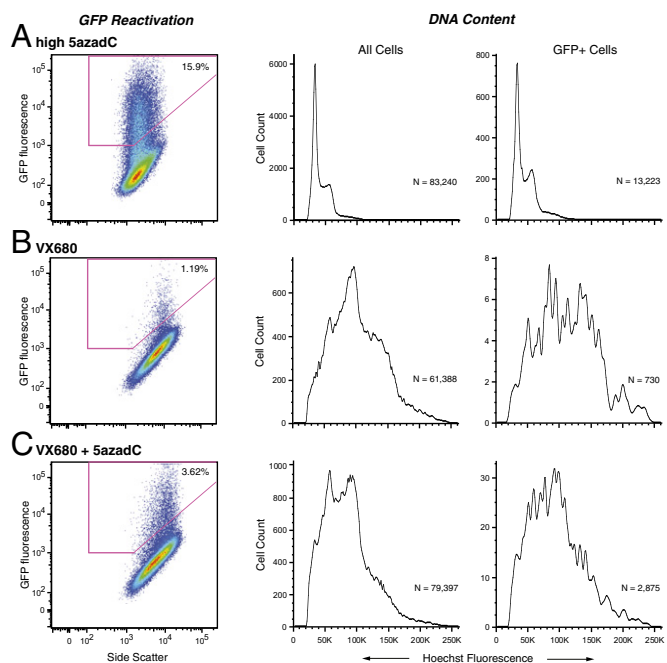


Fig. 4. GFP reactivation as a function of DNA content, shown by FACS. Xi-TgGFP cells were treated for 3 d with (A) 5 μ M 5azadC, (B) 1 μ M VX680, or (C) 1 μ M VX680 + 0.5 μ M 5azadC and subject to FACS analysis. (Left) Gating for GFP⁺ cells, after initial gating (Methods). The x axes, side scatter (log scale); y axes, GFP fluorescent signal (log scale). The percent of GFP⁺ cells is indicated at Top Right. (Center) Histogram of DNA content for all cells at Left. The x axes, Hoechst fluorescence (note that ploidy is on linear scale); y axes, cell count. The number of cells is indicated at Bottom Right. (Right) Histogram of DNA content for GFP⁺ cells at Left. The x axes, Hoechst fluorescence; y axes, cell count. The number of GFP⁺ cells is indicated at Bottom Right.

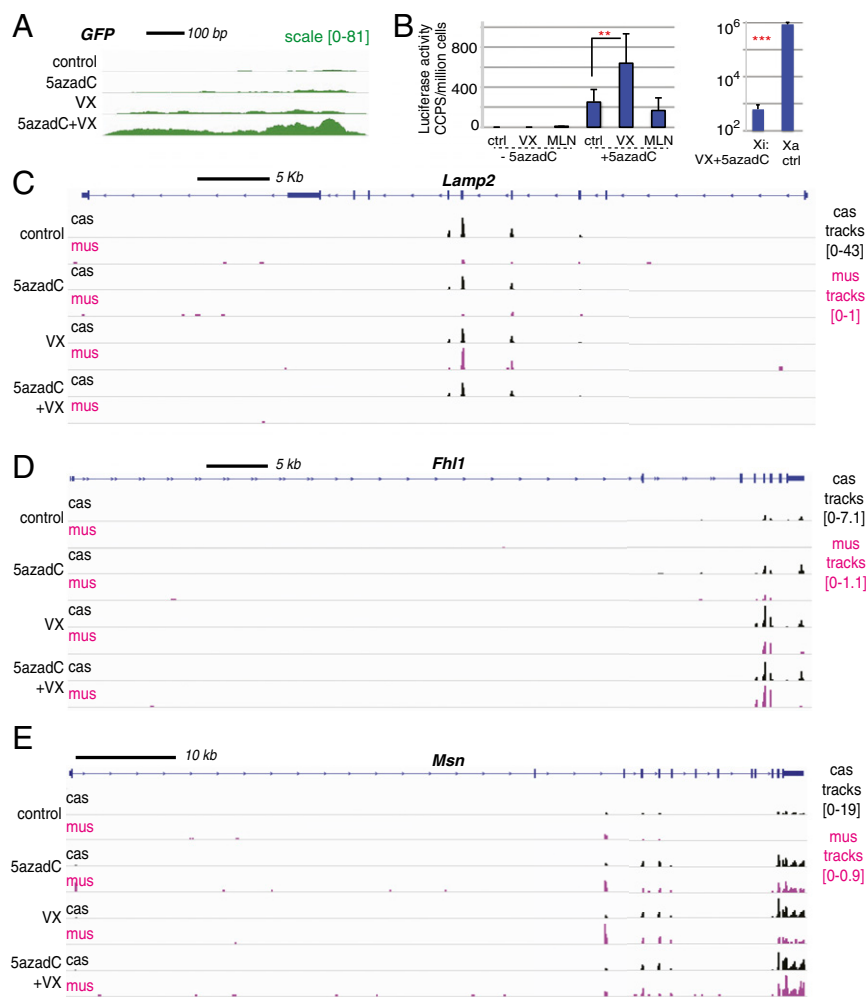


Fig. 5. Allele-specific analysis of X-linked gene expression. (A) RNA-seq, GFP aligned with its cDNA sequence. (B) *Mecp2* expression assayed by luciferase. (Left) Normalized activity from Xi-linked *Mecp2-Luc* (Xi-8 cell line) after 3-d treatment with 1 μ M VX680 (VX) or 1 μ M MLN8237 (MLN) treatments \pm 0.5 μ M 5azadC. Ctrl, control (DMSO) treatment. (Right) Comparison with a control line, Xa-3, where *Mecp2-Luc* is on the Xa (note logarithmic scale). Error bars indicate SD. Means of at least three biological replicates are shown. $**P = 0.01$ ($P \leq 0.005$ for 5azadC, 5azadC + VX, and 5azadC + MLN each compared with the control without 5azadC.) $***P = 4.4 \times 10^{-5}$. (C) *Lamp2*, (D) *Fhl1*, and (E) *Msn* aligned with mm9 in IGV (Top track for each panel). Note that, for the allelic analysis, reads appear only where there are polymorphisms that enable distinction between *cas* (Xa) and *mus* (Xi). For B–D, normalized *cas* and *mus* reads are shown. The scale is indicated at Right; note that it is smaller for *mus* reads. Xi-TgGFP cells were treated as indicated: 5azadC, VX680 (VX), or 5azadC + VX680 as in Fig. 2.

number of Xist RNA clouds. By performing DNA FISH to detect the GFP transgenic locus, control cells, which were tetraploid due to immortalization with SV40 large T antigen, showed an average of 1.9 ± 0.75 Xi per cell ($n = 158$), whereas VX680-treated cells showed 7.6 ± 5.2 Xi per cell ($n = 58$) (Fig. 3C). There was, however, no qualitative difference in the Xist clouds of the control and VX680-treated cells, with Xist properly colocalizing with the GFP transgene probe for both. We also examined steady-state Xist RNA levels by qRT-PCR (Fig. 3D). Nonsignificant differences were observed ($P = 0.07$); however, the downward trend in *Xist* expression upon drug treatment was confirmed by RNA sequencing (RNA-seq) (Fig. 3D and Fig. S2, and see below), which showed Xist levels at between 45% (5azadC only) and 53% (5azadC + VX680) of the control samples.

We then examined the DNA content of treated Xi-TgGFP cells by FACS. Whereas most 5azadC-treated cells fell within peaks corresponding to stages G1 and G2 of mitosis (Fig. 4A, Center; ~33K and 55K on *x* axis), VX680-treated cells had higher DNA content on average and a wider range of ploidies (Fig. 4B, Center, and C, Center). Gating for GFP⁺ cells using side scatter (SSC) vs. GFP fluorescence corrected for the increased autofluorescence of

the VX680-treated cells (Fig. 4, Left, Fig. S3, and Methods). Treatment with 5 μ M 5azadC resulted in 15.9% GFP⁺ cells (Fig. 4A, Left), compared with 0.0021% GFP⁺ mock-treated cells and 0.40% GFP⁺ 0.5 μ M 5azadC-treated cells (Fig. S3). After 1 μ M VX680 treatment, 1.19% of the cells were GFP⁺ (Fig. 4B, Left). The combination of 0.5 μ M 5azadC and 1 μ M VX680 again proved synergistic for GFP reactivation, with 3.62% of treated cells GFP⁺ (Fig. 4C, Left). We next asked whether VX680-treated GFP⁺ cells skewed toward higher DNA content, which would suggest that aneuploidy played a significant role in GFP reactivation. Notably, DNA content of GFP⁺ cells was very similar to the profile of all cells after VX680 treatment (Fig. 4B, Center and Right, and C, Center and Right). Most of these cells were not GFP⁺ despite having DNA content much greater than nontreated or 5azadC-treated cells. Collectively, our data show that GFP reactivation observed with VX680 treatment is unlikely to be due to aneuploidy. Furthermore, the modest reduction in Xist expression does not perturb localization to the Xi.

Reactivation of Native Xi Genes. To further explore the effects of 5azadC and VX680 on native X-linked genes, we performed

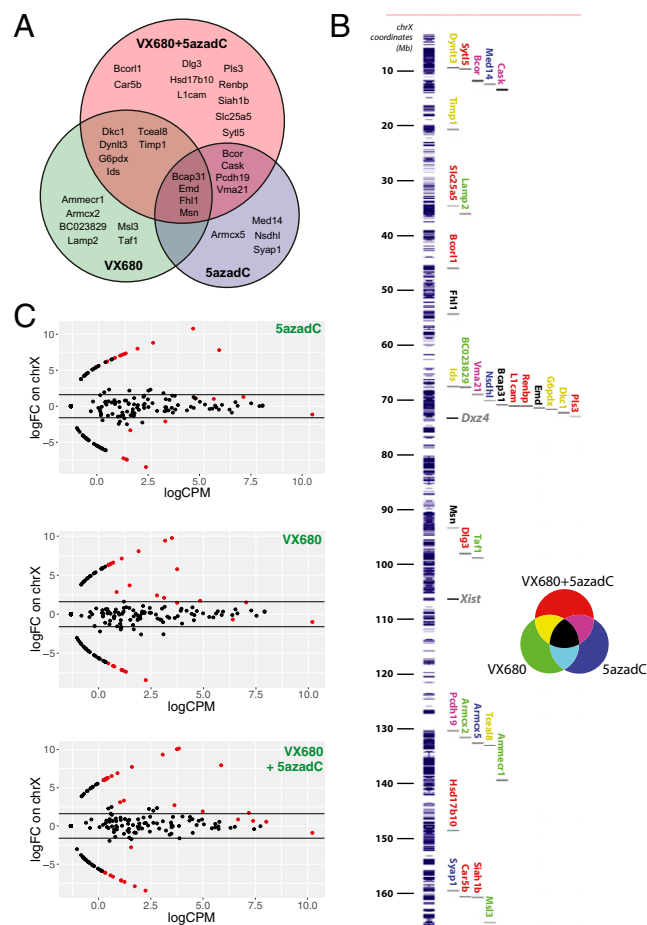


Fig. 6. Reactivated genes on the Xi due to compound treatments. (A) Venn diagram of reactivated Xi-linked genes following indicated treatment. Expression of each gene increased at least threefold with an FDR of <0.05. (B) Distribution of reactivated genes along the Xi. Nucleotide coordinates in megabases are indicated at *Left*; X-linked RefSeq genes are in blue to the *Right* of the coordinates. Of these, reactivated genes are named with the color indicated by the small Venn diagram. Locations of *Dxz4* and *Xist* are indicated in gray. (C) RNA-seq results summarized for the three compound treatments for the Xi (*mus* alleles). In each panel, log₂(fold-change of drug treatment vs. control) on the y axis is plotted against average expression levels across the samples, expressed as log₂(counts per million) on the x axis. Each dot represents one gene. Red dots represent genes where the log₂(fold-change) is significant (FDR < 0.05); the black lines represent a threshold of a threefold change in either direction, i.e., log₂(fold-change) > 1.6 or < -1.6.

qRT-PCR and RNA-seq after treatment with these compounds (Fig. 5 *A–E*). A set of ~250 X-linked genes that met minimum expression levels was considered for each condition. Because the Xi-TgGFP fibroblasts were derived from an F1 hybrid cross of *Mus musculus* and *Mus musculus castaneus* parents, we could analyze the data in an allele-specific manner using the >600,000 X-linked single-nucleotide polymorphisms that occur between the strains; the Xa was invariably of *castaneus* origin (*cas*) and the Xi of *musculus* origin (*mus*) (35). We confirmed reactivation of GFP on the Xi and the synergistic effect of combining 5azadC and VX680 (Fig. 5*A*). For native genes, we observed several patterns, with reactivation defined as at least a threefold increase over the control level that was statistically significant (FDR < 0.05). Some Xi-linked genes were affected by just one compound. For example, mediator complex subunit 14 (*Med14*) was up-regulated by 5azadC only, whereas lysosome-associated membrane protein 2 (*Lamp2*) was reactivated by VX680 only; neither was

reactivated by the combination (Fig. 5*C* and Fig. S4). Meanwhile, for four-and-a-half LIM domains protein 1 (*Fhl1*) (Fig. 5*D*) and moesin (*Msn*) (Fig. 5*E*), the combination treatment resulted in a synergistic boost of expression from the Xi. We also observed up-regulation from the Xa (*cas*) allele in several cases, including *Fhl1*, *Msn*, and solute carrier family 25 member 5 (*Slc25a5*) (Fig. S4).

Changes in expression of the Rett syndrome disease gene, *Mecp2*, were not detected by RNA-seq. We therefore turned to a more sensitive system, using a mouse fibroblast clonal cell line with a luciferase reporter knocked into the endogenous *Mecp2* locus. Xi-8 cells contain this reporter on the Xi. We found that 5azadC incubation resulted in measurable *Mecp2* reactivation, and the addition of VX680, but not MLN8237, enhanced this reactivation significantly (Fig. 5*B*). This activity, however, was three orders of magnitude less than Xa-linked *Mecp2-Luc* activity (Xa-3 cells; Fig. 5*B*). Longer treatment with 5azadC + VX680 or MLN8237 at lower concentrations did not lead to significant increase over 5azadC alone (Fig. S5).

Whereas most Xi genes were not changed by more than two- to threefold either up or down, some 12 to 24 genes on the Xi were reactivated by at least threefold with an FDR of <0.05, upon treatment with 5azadC, VX680, or their combination (Fig. 6). We compared Xi linked to autosomal responses (Fig. 6*C* and Fig. S6). Chr13 is of similar size to the X chromosome and also showed upward and downward gene expression changes of the *mus* allele after treatment (Fig. S6). However, Xi genes showed a greater overall magnitude of fold change compared with Chr13 genes (*mus* allele), both considering all genes on each chromosome, or only those on each with a significant change (Fig. S6). Taken together, our data demonstrate that different treatments elicited reactivation of distinct sets of Xi genes, raising the possibility that defined drugs could be tailored to select genes or regions on the Xi.

Discussion

Our work demonstrates that treatment of female cells with inhibitors of DNA methylation (DNMT) and Aurora kinases leads to a synergistic reactivation of select genes on the Xi. The DNA methyltransferase inhibitor 5azadC has long been known to have a small but significant effect on reactivating the Xi. Here we show that it can do so synergistically with two Aurora kinase inhibitors. We find that when the endogenous genes of the Xi are considered as a whole, three different compound treatments (5azadC alone, VX680 alone, or 5azadC + VX680) reactivate distinct subsets of genes on the Xi. The affected genes are distributed across the length of the X chromosome (Fig. 6*B*); interestingly, a cluster of 11 reactivated genes is located adjacent to the macrosatellite locus DXZ4, a boundary that separates two large megadomains of the Xi (15, 36, 37).

Whereas we do not fully understand the mechanisms of reactivation, our data suggest several factors may be in play. First, we observe that drug treatment results in a 50% down-regulation of Xist RNA levels (Fig. 3*D* and Fig. S2). Although Xist localization is unaffected, the reduced levels could potentially play a role in Xi reactivation. Reduced Xist levels were also observed by Bhatnagar et al. (22) upon knockdown of *Aurka*. The action of 5azadC on DNA methylation and derepression of Xi genes is well established (18, 38); however, its synergism with Aurora kinase inhibition has not been previously reported. Our data indicate that direct inhibition of AURKA and AURKB contribute to reactivation, as knockdown of both *Aurka* and *Aurkb* accounts for some but not all of the GFP reactivation resulting from VX680 or MLN8237 treatment (Fig. 2*C*). Our data are consistent with recent findings regarding the Aurora kinases for maintaining silencing of the Xi. In the findings of Bhatnagar et al. (22), shRNAs targeting *Aurka* resulted in reactivation of various X-linked genes without obvious aneuploidy. AURKB was also pulled down as a protein associating with Xist RNA (15), and its inhibition in combination with 5azadC and etoposide treatments resulted in a synergistic reactivation of Xi genes. AURKB has also been implicated in regulating XIST RNA

adherence to the Xi in human cells undergoing mitosis (39). Significantly, our unbiased approach via a high-throughput screening assay independently identified AURKA and AURKB as relevant targets.

Beyond the finding that the DNA methylation and Aurora kinase pathways act in suppressing the Xi, it is clear that application of VX680 or MLN8237 would be toxic as a therapeutic in the setting of mitotically active cells. Future efforts toward developing a drug based on the synergy between DNMT1 and the Aurora kinases must tease apart the Xi-reactivation effects of VX680/MLN8237 from the effects on the cell cycle. Tests in nondividing cells, such as neurons, would be of particular interest for neurological disorders such as Rett syndrome. Evidence that the Xi reactivation is distinct from cell cycle effects includes the fact that VX680 and MLN8237 both affect the cell cycle, but their effects on Xi reactivation are not identical. It is possible that other kinases inhibited by VX680 and MLN8237 contribute to the reactivation that may not be cell cycle dependent (Table S2) (30, 32). In the future, it may also be possible to use medicinal chemistry to enhance VX680's Xi-reactivation potential while reducing the effects on cell cycle and other pathways.

Methods

Work involving mice adhered to the guidelines of the Massachusetts General Hospital Institutional Animal Care and Use Committee (IACUC) protocol

no. 2004N000100. Immortalized Xi-GFP tail tip fibroblasts (TTFs) for screening were derived from a cross between a *M. musculus* strain carrying an X-linked GFP marker (24) and a *M. m. castaneus* WT mouse. The high-throughput small molecule screen was performed on the Thermo CRS Catalyst Express with automated high-content imaging via ImageXpress Micro. FISH to Xist RNA was performed as described (40). Knockdowns of *Aurka* and *Aurkb* were performed using siRNAs from Dharmacon lipofected into Xi-TgGFP fibroblasts. FACS was performed on the BD LSR II and results were analyzed using FlowJo. RNA-seq analysis was performed as previously described (15) on two biological replicates. Details can be found in *SI Methods*.

ACKNOWLEDGMENTS. We thank D. Dombkowski for assistance with FACS (Massachusetts General Hospital Pathology Flow Cytometry Core), H. Sunwoo for Xist probes and FISH advice, Y. Jeon for control fibroblasts, P. Shinn and D. van Leer for assistance with compound management, and Stuart L. Schreiber and Nicola Tolliday for support as part of the Molecular Libraries Program (1 U54 HG005032-01). We acknowledge the following funding: the Rett Syndrome Research Trust (J.T.L., M.S.B., and A.B.), NIH Grants R03-MH097478 and R01-DA36895 (to J.T.L.), National Center for Research Resources Grant 1510RR023440-01, the Human Frontier Science Program (B.P.), Charles King Postdoctoral Fellowships (to B.P.), the Fund for Scientific Research–Flanders, and the Belgian American Educational Foundation and Plateforme pour l'Éducation et le Talent (L.L.G.C.). A.J., D.J.M., and A. Simeonov were supported by the National Center for Advancing Translational Sciences and the Molecular Libraries Initiative of the NIH Roadmap for Medical Research (U54MH084681). J.T.L. is an Investigator of the Howard Hughes Medical Institute.

1. Starmer J, Magnuson T (2009) A new model for random X chromosome inactivation. *Development* 136(1):1–10.
2. Lee JT (2011) Gracefully ageing at 50, X-chromosome inactivation becomes a paradigm for RNA and chromatin control. *Nat Rev Mol Cell Biol* 12(12):815–826.
3. Distel CM (2012) Dosage compensation of the sex chromosomes. *Annu Rev Genet* 46:537–560.
4. Payer B, Lee JT (2008) X chromosome dosage compensation: How mammals keep the balance. *Annu Rev Genet* 42:733–772.
5. Lifschytz E, Lindsley DL (1972) The role of X-chromosome inactivation during spermatogenesis (Drosophila-allocy-cy-chromosome evolution-male sterility-dosage compensation). *Proc Natl Acad Sci USA* 69(1):182–186.
6. Takagi N, Sasaki M (1975) Preferential inactivation of the paternally derived X chromosome in the extraembryonic membranes of the mouse. *Nature* 256(5519):640–642.
7. Mak W, et al. (2004) Reactivation of the paternal X chromosome in early mouse embryos. *Science* 303(5658):666–669.
8. Ohhata T, Senner CE, Hemberger M, Wutz A (2011) Lineage-specific function of the noncoding Tsix RNA for Xist repression and Xi reactivation in mice. *Genes Dev* 25(16):1702–1715.
9. Payer B, Lee JT, Namekawa SH (2011) X-inactivation and X-reactivation: Epigenetic hallmarks of mammalian reproduction and pluripotent stem cells. *Hum Genet* 130(2):265–280.
10. Payer B, et al. (2013) Tsix RNA and the germline factor, PRDM14, link X reactivation and stem cell reprogramming. *Mol Cell* 52(6):805–818.
11. Monk M, Harper MI (1979) Sequential X chromosome inactivation coupled with cellular differentiation in early mouse embryos. *Nature* 281(5729):311–313.
12. Brown CJ, et al. (1992) The human XIST gene: Analysis of a 17 kb inactive X-specific RNA that contains conserved repeats and is highly localized within the nucleus. *Cell* 71(3):527–542.
13. Wang J, et al. (2001) Imprinted X inactivation maintained by a mouse Polycomb group gene. *Nat Genet* 28(4):371–375.
14. Zhao J, Sun BK, Erwin JA, Song JJ, Lee JT (2008) Polycomb proteins targeted by a short repeat RNA to the mouse X chromosome. *Science* 322(5902):750–756.
15. Minajigi A, et al. (2015) Chromosomes. A comprehensive Xist interactome reveals cohesin repulsion and an RNA-directed chromosome conformation. *Science* 349(6245):aab2276.
16. Sugimoto M, Abe K (2007) X chromosome reactivation initiates in nascent primordial germ cells in mice. *PLoS Genet* 3(7):e116.
17. Chuva de Sousa Lopes SM, et al. (2008) X chromosome activity in mouse XX primordial germ cells. *PLoS Genet* 4(2):e30.
18. Csankovszki G, Nagy A, Jaenisch R (2001) Synergism of Xist RNA, DNA methylation, and histone hypoacetylation in maintaining X chromosome inactivation. *J Cell Biol* 153(4):773–784.
19. McGraw CM, Samaco RC, Zoghbi HY (2011) Adult neural function requires MeCP2. *Science* 333(6039):186.
20. Kilstrup-Nielsen C, et al. (2012) What we know and would like to know about CDKL5 and its involvement in epileptic encephalopathy. *Neural Plast* 2012:728267.
21. Chan KM, Zhang H, Malureanu L, van Deursen J, Zhang Z (2011) Diverse factors are involved in maintaining X chromosome inactivation. *Proc Natl Acad Sci USA* 108(40):16699–16704.
22. Bhatnagar S, et al. (2014) Genetic and pharmacological reactivation of the mammalian inactive X chromosome. *Proc Natl Acad Sci USA* 111(35):12591–8.
23. Minkovsky A, et al. (2015) A high-throughput screen of inactive X chromosome reactivation identifies the enhancement of DNA demethylation by 5-aza-2'-dC upon inhibition of ribonucleotide reductase. *Epigenetics Chromatin* 8:42.
24. Hadjantonakis AK, Cox LL, Tam PP, Nagy A (2001) An X-linked GFP transgene reveals unexpected paternal X-chromosome activity in trophoblastic giant cells of the mouse placenta. *Genesis* 29(3):133–140.
25. Harrington EA, et al. (2004) VX-680, a potent and selective small-molecule inhibitor of the Aurora kinases, suppresses tumor growth in vivo. *Nat Med* 10(3):262–267.
26. Nair JS, Schwartz GK (2016) MLN-8237: A dual inhibitor of aurora A and B in soft tissue sarcomas. *Oncotarget* 7(11):12893–12903.
27. Fu J, Bian M, Jiang Q, Zhang C (2007) Roles of Aurora kinases in mitosis and tumorigenesis. *Mol Cancer Res* 5(1):1–10.
28. Manfredi MG, et al. (2011) Characterization of Alisertib (MLN8237), an investigational small-molecule inhibitor of aurora A kinase using novel in vivo pharmacodynamic assays. *Clin Cancer Res* 17(24):7614–7624.
29. Tyler RK, Shpiro N, Marquez R, Evers PA (2007) VX-680 inhibits Aurora A and Aurora B kinase activity in human cells. *Cell Cycle* 6(22):2846–2854.
30. Bain J, et al. (2007) The selectivity of protein kinase inhibitors: A further update. *Biochem J* 408(3):297–315.
31. Karaman MW, et al. (2008) A quantitative analysis of kinase inhibitor selectivity. *Nat Biotechnol* 26(1):127–132.
32. Davis MI, et al. (2011) Comprehensive analysis of kinase inhibitor selectivity. *Nat Biotechnol* 29(11):1046–1051.
33. Goldenson B, Crispino JD (2015) The aurora kinases in cell cycle and leukemia. *Oncogene* 34(5):537–545.
34. Hégarat N, et al. (2011) Aurora A and Aurora B jointly coordinate chromosome segregation and anaphase microtubule dynamics. *J Cell Biol* 195(7):1103–1113.
35. Pinter SF, et al. (2012) Spreading of X chromosome inactivation via a hierarchy of defined Polycomb stations. *Genome Res* 22(10):1864–1876.
36. Horakova AH, Moseley SC, McLaughlin CR, Tremblay DC, Chadwick BP (2012) The macrosatellite DXZ4 mediates CTCF-dependent long-range intrachromosomal interactions on the human inactive X chromosome. *Hum Mol Genet* 21(20):4367–4377.
37. Rao SS, et al. (2014) A 3D map of the human genome at kilobase resolution reveals principles of chromatin looping. *Cell* 159(7):1665–1680.
38. Riggs AD (2002) X chromosome inactivation, differentiation, and DNA methylation revisited, with a tribute to Susumu Ohno. *Cytogenet Genome Res* 99(1–4):17–24.
39. Hall LL, Byron M, Pageau G, Lawrence JB (2009) AURKB-mediated effects on chromatin regulate binding versus release of XIST RNA to the inactive chromosome. *J Cell Biol* 186(4):491–507.
40. Zhang L-F, Huynh KD, Lee JT (2007) Perinucleolar targeting of the inactive X during S phase: Evidence for a role in the maintenance of silencing. *Cell* 129(4):693–706.
41. Wang J, et al. (2015) Wild-type microglia do not reverse pathology in mouse models of Rett syndrome. *Nature* 521(7552):E1–E4.
42. Ingles J, et al. (2007) High-throughput screening assays for the identification of chemical probes. *Nat Chem Biol* 3(8):466–479.
43. Pinter SF, et al. (2015) Allelic imbalance is a prevalent and tissue-specific feature of the mouse transcriptome. *Genetics* 200(2):537–549.
44. Lee JT, Lu N (1999) Targeted mutagenesis of Tsix leads to nonrandom X inactivation. *Cell* 99(1):47–57.
45. Heinz S, et al. (2010) Simple combinations of lineage-determining transcription factors prime cis-regulatory elements required for macrophage and B cell identities. *Mol Cell* 38(4):576–589.
46. Robinson MD, McCarthy DJ, Smyth GK (2010) edgeR: A Bioconductor package for differential expression analysis of digital gene expression data. *Bioinformatics* 26(1):139–140.
47. Wickham H (2009) *ggplot2: Elegant Graphics for Data Analysis* (Springer, New York).